Sub-pixel processing algorithm of the reducing boundary recursive error in staring FPA micro-scanning imaging

Yan Chen (陈 艳)*, Weiqi Jin (金伟其), Lingxue Wang (王岭雪), and Xia Wang (王 霞)

School of Optoelectronics, Beijing Institute of Technology, Beijing 100081, China

**E-mail: chenyan340206@yahoo.com.cn*

Received April 24, 2009

By analyzing the error distribution rule of the boundary recursive reconstruction algorithm in controlled micro-scanning, a sub-pixel image processing algorithm is proposed to reduce the error. The gray statistical principle is used in the algorithm to optimize the error and acquire the sub-pixel image that approximates the original image. The simulation result shows that the effect of this algorithm is better than the over-sample and simple boundary recursive algorithm (BRA), and it results in a good effect both in those of visible light and infrared imaging systems. Therefore, the application of this algorithm will enhance the performance of optoelectronic imaging systems.

OCIS codes: 110.4155, 100.3008, 100.3020, 100.2000.

doi: 10.3788/COL20100802.0146.

In the discrete optoelectronic imaging device, the detector affects the system imaging quality because of the unclear imaging caused by the large size of the detector and the under-sampling caused by the large discrete sampling space intervals. The system resolution can be effectively improved by decreasing the detector unit size and increasing the detector duty ratio. However, these methods are limited by detector technique, sensitivity, optical system diffraction limit, and the device cost. It is demonstrated that optical micro-scanning and later image processing can decrease the under-sampling effect with high performance-price ratio, and it has become a feasible way to develop a high-performance optoelectronic image system. This technology has been applied successfully in the fields of remote sensing, thermal imaging, and microscopy imaging[1−3].

The sub-pixel imaging technology based on micro-scanning controls the imaging process by optical micro-scanning, and combines with later sub-pixel image processing to obtain a space resolution smaller than the size of the detector. This technology has been used in line scanning and area staring focal plane array (FPA) imaging fields, and its key step is processing the boundary issue. Many current algorithms do not consider the boundary issue and stay only at over-sampling imaging, which means that they are not really sub-pixel imaging[4]. Jin *et al.* discussed the boundary issue in 288 × 4 scanning thermal imaging system, and put forward the boundary recursive algorithm (BRA)[5]. This algorithm results in certain effects, but it introduces the error of positive-negative alternating. Based on Ref. [5], Gao *et al.* dealt with the error using the gray statistical principle, and then greatly improved the image resolution[6]. Xu *et al.* introduced the BRA to two-dimensional (2D) staring FPA imaging and realized accurate sub-pixel imaging[7], but it needs setting fixed boundary or embedded blackbody at the field diaphragm to keep uniformity of the boundary, which was very difficult to realize in a real system. Considering of this difficulty, the method in this letter will not deal with the field diaphragm, and just analyze the error distribution rule of BRA in 2D staring FPA imaging, and then put forward a sub-pixel image processing algorithm that can reduce the error.

According to the order of scanning, controlled micro-scanning had many models, such as 1 × 1, 2 × 2, 3 × 3, 4 × 4, and so on[8,9]. Figure 1 takes the 2 × 2 model to interpret the over-sampling reconstruction of the controlled micro-scanning. Keeping the imaging scene invariable makes the FPA move one half of the unit detector to the right, down, and left, respectively, relative to the target scene and, gains four under-sampling images A, B, C, and D. As shown in Fig. 2, the four under-sampling images are interpolated according to the sampling order to create the over-sampling image P. The space sampling rate is improved, so the over-sampling image P contains more target scene information, which can improve the image detail resolution.

In Fig. 2, we note that the over-sampling image P and the original image O have the following relationship[10]

$$\begin{aligned} P(i,j) =&[O(i,j)+O(i,j+1) \\ &+O(i+1,j)+O(i+1,j+1)]/4 \\ &(i=1,2,\cdots,2m; j=1,2,\cdots,2n). \end{aligned} \quad (1)$$

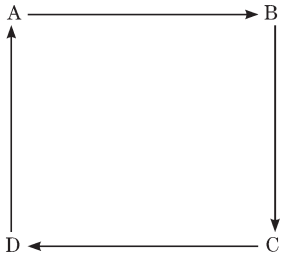

Fig. 1. Working model of 2 × 2 controlled micro-scanning.

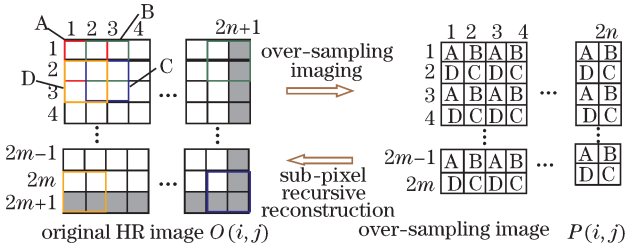

Fig. 2. Reconstruction of the over-sampling image.

Equation (1) can be rewritten in a matrix form as

$$\mathbf{P}_1 = \frac{1}{4}(\mathbf{W}\mathbf{O}_1 + \mathbf{O}'), \tag{2}$$

where $\mathbf{P}_1$ is $(2m\times2n) \times 1$ column vector, which is expanded from image $P(i,j)$ in the order of rows and columns. That is, $\mathbf{P}_1[2n \times (i–1)+j] = P(i,j)$, $\mathbf{O}_1$ is $(2m\times2n) \times 1$ column vector coming from $O(i,j)$: $\mathbf{O}_1[2n\times (i–1)+j] = O(i,j)$, and $\mathbf{O}'$ is $(2m\times2n) \times 1$ column vector reconstructed from the values of $(2m+1)$ row and $(2n+1)$ column of image $O(i,j)$ by

$$\begin{aligned} O' =&[\overbrace{0\cdots0}^{2n-1}, O(1,2n+1)+O(2,2n+1),\cdots,\overbrace{0\cdots0}^{2n-1},\\ &O(i,2n+1)+O(i+1,2n+1),\cdots,\overbrace{0\cdots0}^{2n-1},\\ &O(2m-1,2n+1)+O(2m,2n+1), O(2m+1,1)\\ &+O(2m+1,2), \cdots, O(2m+1,j)+O(2m+1,j+1),\\ &\cdots, O(2m+1,2n-1)+O(2m+1,2n),\\ &O(2m,2n+1)+O(2m+1,2n)\\ &+O(2m+1,2n+1)]^{\mathrm{T}}. \end{aligned} \tag{3}$$

The transposition matrix $\mathbf{W}$ is composed of $2m\times2n$ submatrices w_r (r = 1, 2,$\cdots$, $2m\times2n$), as reprsented in

$$\mathbf{W} = \left[w_1, w_2, \cdots, w_r, \cdots, w_{2m\times(2n-1)}, w_{2m\times2n}\right]^{\mathrm{T}}_{4m^2\times4n^2}, \tag{4}$$

$$w_r = \begin{cases} [\ \overbrace{0\cdots0}^{r-1}1\overbrace{00\cdots0}^{2n-1}1\ \overbrace{00\cdots\cdots0}^{2m\times2n-2n-r}\ ]_{1\times(2m\times2n)}, \\ \quad r = 2tn, t = 1, 2, 3, \cdots, 2m-1, \\ [\ \overbrace{0\cdots0}^{r-1}11\overbrace{00\cdots0}^{2n-2}11\ \overbrace{00\cdots\cdots0}^{2m\times2n-2n-r-1}\ ]_{1\times(2m\times2n)}, \\ \quad \text{other}. \end{cases} \tag{5}$$

It can be seen that the transposition matrix $\mathbf{W}$ is an upper diagonal matrix, and the diagonal elements are not zeros, so its inverse matrix exists. Then from Eq. (2), we have

$$\mathbf{O}_1 = \mathbf{W}^{-1}(4\mathbf{P}_1 - \mathbf{O}'). \tag{6}$$

Although Eq. (6) has proven the feasibility of sub-pixel processing, it requires a large computation load and large memory capacity. Therefore, it is difficult to implement. According to Eq. (1), Eq. (6) can be rewritten in the recursive form:

$$\begin{aligned} &O(2m-k,2n-l) = 4P(2m-k,2n-l)\\ &-O(2m-k,2n-l+1)-O(2m-k+1,2n-l)\\ &-O(2m-k+1,2n-l+1)(k=0,1,2,\cdots,\\ &2m-1; l=0,1,2,\cdots,2n-1), \end{aligned} \tag{7}$$

that is, if the matrix $\mathbf{O}'$ is known beforehand, O can be obtained from the over-sampling image P. Although the matrix $\mathbf{O}'$ can be ascertained accurately by setting fixed boundary or embedded blackbody at the field diaphragm, it is difficult to implement in practice. In most cases, the image gray value does not always change fast. Therefore, it can be assumed that the pixel values of $2m$ row and $2n$ column of over-sampling image P equal approximately the corresponding pixel values of $(2m+1)$ row and $(2n+1)$ column of image O, that is

$$\begin{aligned} O(i,2n+1) &\approx P(i,2n), O(2m+1,j)\\ &\approx P(2m,j), O(2m+1,2n+1)\\ &\approx P(2m,2n). \end{aligned} \tag{8}$$

Substituting Eq. (8) into Eq. (7), the reconstructive image OO is obtained as

$$\begin{cases} OO(2m,2n) = P(2m,2n),\\ OO(2m-k,2n) = 3P(2m-k,2n)\\ \quad -OO(2m-k+1,2n)-P(2m-k+1,2n),\\ OO(2m,2n-l) = 3P(2m,2n-l)\\ \quad -OO(2m,2n-l+1)-P(2m,2n-l+1),\\ OO(2m-k,2n-l) = 4P(2m-k,2n-l)\\ \quad -OO(2m-k,2n-l+1)-OO(2m-k+1,2n-l)\\ \quad -OO(2m-k+1,2n-l+1),\\ \quad (k=1,2\cdots2m-1;\ l=1,2\cdots2n-1). \end{cases} \tag{9}$$

In Eq. (8), $2m$ row and the $2n$ column of P are used to replace the boundary pixels of the original high resolution (HR) image O, thus the OO from Eq. (7) has some error as compared with the original image O. The key step of obtaining the HR image is the analysis and optimization of the error.

The $2m$ row and $2n$ column pixels of P are not equal to the corresponding boundary pixels of O, so between them, there exist some error as follows:

$$\begin{aligned} O\,(2m-k,2n+1) &= P\,(2m-k,2n)+\beta_{\text{2m-k}},\\ O\,(2m+1,2n-l) &= P\,(2m,2n-l)+\alpha_{\text{2n-l}},\\ O\,(2m+1,2n+1) &= P\,(2m,2n)+\gamma,\\ (k=0,\cdots,2m-1; l=0,\cdots,2n-1). & \end{aligned} \tag{10}$$

Taking Eq. (10) into Eq. (7), the original HR image O can be obtained as

$$\begin{cases} O(2m,2n) = P(2m,2n)-(\alpha_{2n}+\beta_{2m}+\gamma)\\ O(2m-k,2n) = 3P(2m-k,2n)-O(2m-k+1,2n)\\ \quad -P(2m-k+1,2n)-(\beta_{2m-k}+\beta_{2m-k+1})\\ O(2m,2n-l) = 3P(2m,2n-l)-O(2m,2n-l+1)\\ \quad -P(2m,2n-l+1)-(\alpha_{2n-l}+\alpha_{2n-l+1})\\ O(2m-k,2n-l) = 4P(2m-k,2n-l)\\ \quad -O(2m-k,2n-l+1)-O(2m-k+1,2n-l)\\ \quad -O(2m-k+1,2n-l+1),\\ \quad (k=1,2,\cdots,2m-1; l=1,2,\cdots,2n-1). \end{cases} \tag{11}$$

The pixels of O are subtracted from the corresponding pixels of OO, or Eq. (11) is subtracted from Eq. (9). The relationship between reconstructive image OO and original image O is

$$OO(i,j) = O(i,j)+(-1)^i(\alpha_j+(-1)^j\gamma)+(-1)^j\beta_i, \tag{12}$$

where $(-1)^i(\alpha_j+(-1)^j\gamma)+(-1)^j\beta_i$ is the corresponding error of every pixel. Its distribution is listed in Table 1. Using the first column as an example, there is an error of positive-negative alternating $(\alpha_1-\gamma)$ in

Table 1. Error Distribution of Boundary Recursive Reconstructive Image *OO*

$-(\alpha_1-\gamma)-\beta_1$	$-(\alpha_2+\gamma)+\beta_1$	$-(\alpha_3-\gamma)-\beta_1$	$-(\alpha_4+\gamma)+\beta_1$	$\cdots$	$-(\alpha_{2n-1}+\gamma)+\beta_1$	$-(\alpha_{2n}+\gamma)+\beta_1$
$(\alpha_1-\gamma)-\beta_2$	$(\alpha_2+\gamma)+\beta_2$	$(\alpha_3-\gamma)-\beta_2$	$(\alpha_4+\gamma)+\beta_2$	$\cdots$	$(\alpha_{2n}+\gamma)+\beta_2$	$(\alpha_{2n}+\gamma)+\beta_2$
$-(\alpha_1-\gamma)-\beta_3$	$-(\alpha_2+\gamma)+\beta_3$	$-(\alpha_3-\gamma)-\beta_3$	$-(\alpha_4+\gamma)+\beta_3$	$\cdots$	$-(\alpha_{2n-1}+\gamma)+\beta_3$	$-(\alpha_{2n}+\gamma)+\beta_3$
$(\alpha_1-\gamma)-\beta_4$	$(\alpha_2+\gamma)+\beta_4$	$(\alpha_3-\gamma)-\beta_4$	$(\alpha_4+\gamma)+\beta_4$	$\cdots$	$(\alpha_{2n}+\gamma)+\beta_4$	$(\alpha_{2n}+\gamma)+\beta_4$
$\vdots$	$\vdots$	$\vdots$	$\vdots$	$\cdots$	$\vdots$	$\vdots$
$-(\alpha_1-\gamma)-\beta_{2m-1}$	$-(\alpha_2+\gamma)+\beta_{2m-1}$	$-(\alpha_3-\gamma)-\beta_{2m-1}$	$-(\alpha_4+\gamma)+\beta_{2m-1}$	$\cdots$	$-(\alpha_{2n-1}+\gamma)+\beta_{2m-1}$	$-(\alpha_{2n}+\gamma)+\beta_{2m-1}$
$(\alpha_1-\gamma)-\beta_{2m}$	$(\alpha_2+\gamma)+\beta_{2m}$	$(\alpha_3-\gamma)-\beta_{2m}$	$(\alpha_4+\gamma)+\beta_{2m}$	$\cdots$	$(\alpha_{2n}+\gamma)+\beta_{2m}$	$(\alpha_{2n}+\gamma)+\beta_{2m}$

the odd and even rows. Summing separately the odd and even rows of OO, we have

$$\begin{cases} \sum\limits_{i=1}^{m} OO(2i-1,1) = \sum\limits_{i=1}^{m} O(2i-1,1) \\ \qquad\qquad - \sum\limits_{i=1}^{m} \beta_{2i-1} - m(\alpha_1-\gamma) \\ \sum\limits_{i=1}^{m} OO(2i,1) = \sum\limits_{i=1}^{m} O(2i,1) - \sum\limits_{i=1}^{m} \beta_{2i} + m(\alpha_1-\gamma)\ . \end{cases} \tag{13}$$

According to the mathematical statistics theory, because $(\sum\limits_{i=1}^{m} O(2i-1,1) - \sum\limits_{i=1}^{m} \beta_{2i-1})$ and $(\sum\limits_{i=1}^{m} O(2i,1) - \sum\limits_{i=1}^{m} \beta_{2i})$ are the sums of large samples, they should be approximately equal. Therefore, the approximate solution of error $(\alpha_1-\gamma)$ from Eq. (13) is

$$(\alpha_1-\gamma)' = \frac{\sum\limits_{i=1}^{m} OO(2i,1) - \sum\limits_{i=1}^{m} OO(2i-1,1)}{2m}. \tag{14}$$

For the same reason, the approximate solutions of errors $(\alpha_j+(-1)^j\gamma)'$ in other columns can likewise be obtained. The experimental results show that the residual error of $(\alpha_j+(-1)^j\gamma)'$ and $(\alpha_j+(-1)^j\gamma)$ is less than 10^{-4}, thus they are approximately equal. After optimizing the error $(\alpha_j+(-1)^j\gamma)$, the reconstructive image $OO1$ is obtained as

$$OO1(i,j) = O(i,j) + (-1)^j\beta_i, \tag{15}$$

where $(-1)^j\beta_i$ is the error of $OO1$ as compared with O. Its distribution is listed in Table 2. There is error of positive-negative alternating β_i in the odd and even columns of each row. According to the gray statistical principle, the approximate solution of β_i is

$$\beta_i' = \frac{\sum\limits_{j=1}^{n} OO1(i,2j) - \sum\limits_{j=1}^{n} OO1(i,2j-1)}{2n}. \tag{16}$$

Table 2. Error Distribution of Image *OO*1

$-\beta_1$	β_1	$-\beta_1$	β_1	$\cdots$	$-\beta_1$	β_1
$-\beta_2$	β_2	$-\beta_2$	β_2	$\cdots$	$-\beta_2$	β_2
$-\beta_3$	β_3	$-\beta_3$	β_3	$\cdots$	$-\beta_3$	β_3
$-\beta_4$	β_4	$-\beta_4$	β_4	$\cdots$	$-\beta_4$	β_4
$\vdots$	$\vdots$	$\vdots$	$\vdots$	$\cdots$	$\vdots$	$\vdots$
$-\beta_{2m-1}$	β_{2m-1}	$-\beta_{2m-1}$	β_{2m-1}	$\cdots$	$-\beta_{2m-1}$	β_{2m-1}
$-\beta_{2m}$	β_{2m}	$-\beta_{2m}$	β_{2m}	$\cdots$	$-\beta_{2m}$	β_{2m}

After optimizing the error β_i, the reconstructive image $OO2$ is obtained by

$$OO2(i,j) = O(i,j) - (-1)^j(\beta_i - \beta_i'). \tag{17}$$

The residual error $(\beta_i - \beta_i')$ is less than 10^{-4}. Therefore, after optimizing the errors $(\alpha_j + (-1)^j\gamma)$ and β_i, the sub-pixel reconstructive image $OO2$ becomes equal to the original image O.

To prove the validity of the sub-pixel processing algorithm in this letter, visual and infrared images with sharp edge are used in the simulation, and the quantification of quality is appraised by the parameters peak signal-to-noise ratio (PSNR)[11] and universal image quality index (Q)[12]. The range of Q is $[-1,1]$, and it is defined by

$$Q = \frac{4\sigma_{xy}\cdot\bar{x}\cdot\bar{y}}{(\sigma_x^2+\sigma_y^2)\cdot[(\bar{x})^2+(\bar{y})^2]}, \tag{18}$$

$$\sigma_x^2 = \frac{1}{MN-1}\sum_{i=1}^{M}\sum_{j=1}^{N}(I_{i,j}-\bar{x})^2,$$

$$\sigma_y^2 = \frac{1}{MN-1}\sum_{i=1}^{M}\sum_{j=1}^{N}(T_{i,j}-\bar{y})^2,$$

$$\sigma_{xy} = \frac{1}{MN-1}\sum_{i=1}^{M}\sum_{j=1}^{N}(I_{i,j}-\bar{x})(T_{i,j}-\bar{y}),$$

$$\bar{x} = \frac{1}{MN}\sum_{i=1}^{M}\sum_{j=1}^{N}I_{i,j}, \bar{y} = \frac{1}{MN}\sum_{i=1}^{M}\sum_{j=1}^{N}T_{i,j}, \tag{19}$$

Where I is the original image, and T is the reconstructed image.

Figure 3 gives the processing effects of visual image liftingbody.bmp (256×256).

Figuer 4 is the error distributions of the three reconstructive algorithms about liftingbody.bmp. It can be seen that the error of the over-sampling image is random. On the other hand, the error of the BRA image is based on rules, and the effect is better than that of the over-sampling image. The error of the sub-pixel image after EO is reduced greatly, and the sub-pixel image is close to the original image.

Although BRA is better than over-sampling in most cases, it is not suitable for all cases, such as in situations in which the boundary pixels of the image vary fast or have many details. In this case, BRA will bring many errors. Figure 5 is the processing effects of the infrared image of jianzhu.bmp (128×128). There is obvious error in BRA as shown in Fig. 5 (c), making it difficult

to discern. However, the error distribution is based on rules, so the gray statistical principle can also be used to optimize the error and then gain the sub-pixel image as shown in Fig. 5(d).

Figure 6 gives the error distribution of these three reconstructive algorithms about jianzhu.bmp. It can be seen that after EO, the error of the sub-pixel image is obviously reduced.

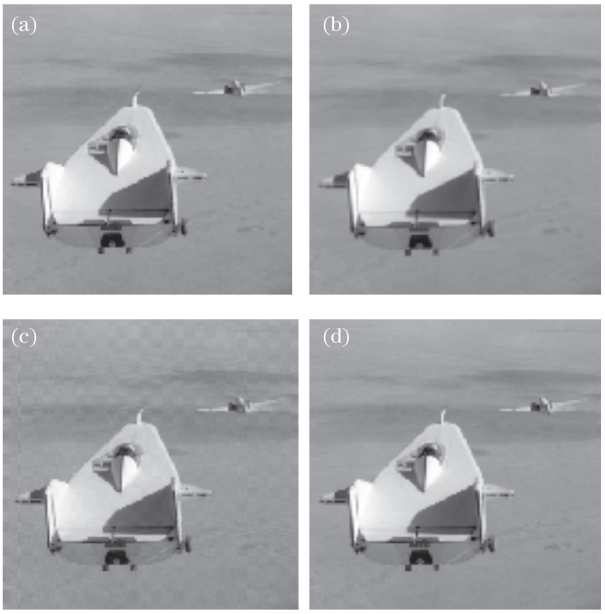

Fig. 3. Processing effects of visual images of liftingbody.bmp (256×256). (a) original HR image O, (b) over-sampling image P gained from Eq. (1), (c) reconstructive image OO by the BRA, and (d) sub-pixel image $OO2$ after error optimization (EO).

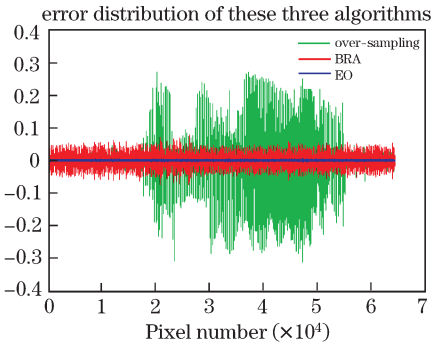

Fig. 4. Error distributions of three algorithms about liftingbody.bmp.

Table 3. Image Evaluating Parameters of the Three Algorithms

Algorithms	Parameters	PSNR	Q
	Over-Sampling	79.7152	0.9767
Liftingbody.bmp	BRA	84.8842	0.9931
	EO	106.4377	1
	Over-Sampling	75.0899	0.9695
Jianzhu.bmp	BRA	73.4262	0.9582
	EO	101.5118	1

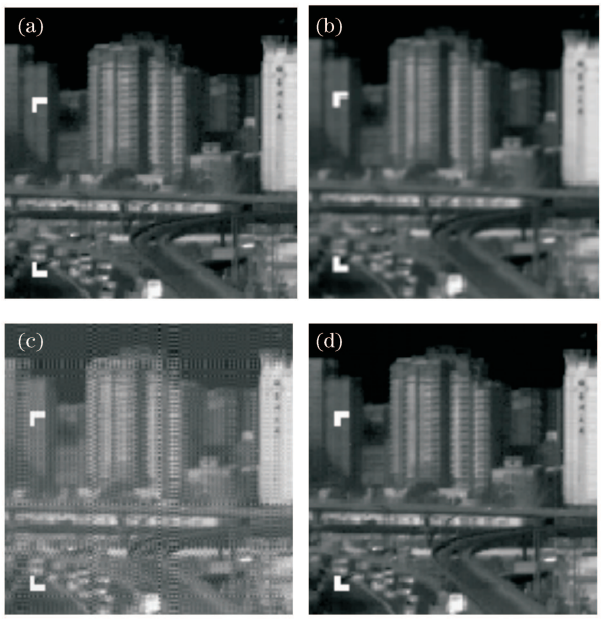

Fig. 5. Processing effects of infrared images of jianzhu.bmp (128×128). (a) original HR image O, (b) over-sampling image P gained from Eq. (1), (c) reconstructive image OO by the BRA, and (d) sub-pixel image $OO2$ after error optimization (EO).

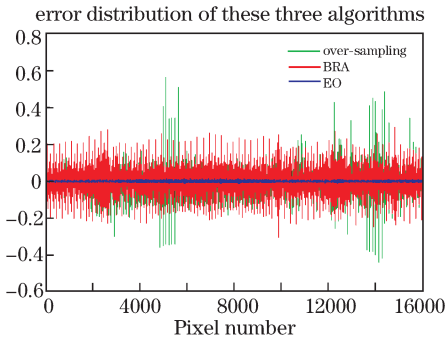

Fig. 6. Error distribution of three algorithms about jianzhu.bmp.

Table 3 shows the evaluating parameters of the reconstructive images about liftingbody.bmp and jianzhu.bmp, and the sub-pixel image quality after EO is greatly improved.

Micro-scanning is an effective way to improve the capability of imaging systems, but it must be combined with later image processing to enhance the development of image quality. By focusing on the issue that BRA can bring error in staring micro-scanning, we analyze the error distribution rule, uses the gray statistical principle to optimize the error, and obtain the sub-pixel image with greatly improved resolution. The simulation result demonstrates that the algorithm used in this letter has a result better effect than the over-sampling algorithm and BRA (regardless of whether it uses visual effect or the evaluating parameters). The algorithm is universal, so it can optimize the error brought by BRA whether the error is great or small. In addition, the algorithm is simple but effective with small processing load (on the PC with AMD 3000 + CPU and 512 MB memory, the time of dealing with a 256×256 image with matlab is

0.1 s), so it may be used in practical applications, and for future uses, it can be extended to uncontrolled micro-scanning situations.

This work was supported by Beijing Micro-Chemical Institute Laboratory Open Fund (No. P2008026EB) and the General Armament Department Fund (No. 40405030103).

References

1. Christophe Latry and Bernard Rouge, Proc. SPIE **3439,** 480 (1998).
2. Jenoptik System, "ProgRes C14plus Technical Data", http://www.jenoptik.com (Apr. 24, 2009).
3. "LION-Lightweight Infrared Observation Nightsight", http://www.thales group-optronics.com (Apr. 24, 2009).
4. X. Wang, F. Hu, J. Zhang, and Z. Feng, Journal of Xdian University (in Chinese) **32,** 3 (2005).
5. W. Jin, C. Wang, N. Zhang, L. Wang, and P. Lu, J. Infrared Millim. Waves (in Chinese) **24,** 261 (2005).
6. B. Gao, "Study on sub-pixel processing algorithm for scanning FPA thermal imaging system without frame" Master Thesis (Beijing Institute of Technology, Beiging 2008).
7. C. Xu, W. Jin, Y. Li, and X. Wang, Acta Electron. Sin. (in Chinese) **35,** 1608 (2007).
8. Y. Zuo and J. Zhang, J. Infrared Millim. Waves (in Chinese) **22,** 146 (2003).
9. H. Wang, S. Liu, D. Wang, and Q. Lu, Acta Opt. Sin. (in Chinese) **29,** 1211 (2009).
10. Y. Li, W. Jin, C. Xu, and X. Wang, Journal of China Ordnance **4,** 259 (2008).
11. G. Chen, K. Yang, R. Chen, and Z. Xie, Chin. Opt. Lett. **6,** 648 (2008).
12. Z. Wang and A. C. Bovik, IEEE Signal Processing Letters **9,** 81 (2002).